Derivation of a Lorentz force generation model on Bearingless surface-mounted PM synchronous motors

Toshie KIKUCHI* and Masahide OOSHIMA*
* Department of Mechanical and Electrical Engeneering, Suwa University of Science
5000-1 Toyohira, Chino-city, Nagano 391-0292, Japan
E-mail: kikuchi_toshie@rs.sus.ac.jp

Abstract
This paper presents the Lorentz force generation model for bearingless Surface-mounted PM Synchronous motors. The Lorentz force varies according to the different combination of pole numbers of the motor windings and the suspension windings of bearingless motor. The mathematical model of bearingless motors with generalized pole number are analyzed. The derived models are compared with FEM simulation using the bearingless motor models with the combination of 2-pole motor and 4-pole suspension windings, 4-pole motor and 2-pole suspension windings , 4-pole motor and 6-pole suspension windings, 6-pole and 4-pole bearingless motors. The analytical model and FEM simulation agree mostly in the y-direction, however, more than 10% error appears in x-direction. From result of the additional investigation, it is considered that the cause of the analytical calculation error is the effect of the reflective magnetic field by the eddy current.

Keywords : Bearingless motors, SPM, Lorentz force, eddy current

1. Introduction

Bearingless motors have been developed and utilized for applications which require suspending a rotational machine without mechanical contact. There is a known condition concerning the motor winding in which the difference in pole numbers in the suspension winding and the motor winding is two (Okada, Dejima and Ohishi, 1995). Rotation speed of the magnetic flux generated by the suspension winding and the motoring winding is different according to the combination of the pole numbers. The surface permanent magnetic synchronous motors (SPM) often have high conductive permanent magnet on the rotor. On the rotor rotational coordinate the magnetic flux by the suspension windings go across the permanent magnet. The time variation of the magnetic flux induces an electromotive force on the permanent magnet. In the case of the permanent magnet is conductive, electromotive force causes the eddy current opposing the variation of the magnetic flux(Fukushima, Ooshima, 2020). The effects by the eddy current to the suspension force originate from two kinds of sources. The first one is that the reflective magnetic field by the eddy current distorts the symmetrical distribution of the air gap flux density. The second one is called Lorentz force produced with the permanent magnetic flux and the eddy current flowing in the perpendicular direction of it. The previous research has proposed the calculation method for the radial suspension force of the bearingless Surface-mounted PM Synchronous motors based on the air gap flux density (Noguchi, Sugimoto, Fujii, Chiba, 2022). In this research, the mathematical model of Lorentz force for the bearingless Surface-mounted PM Synchronous motors in which the pole number is considered as a parameter is newly derived based on the flux density distribution. The validity of the derived model is confirmed by the FEM simulation including the combinations of 2-pole and 4-pole, and 6-pole and 4-pole.

2. Derivation of Lorentz force

2.1. Eddy current induced by the magnetic suspension flux

Firstly, the rotor position definitions and the stational reference frame used in this research are explained with refering to Fig. 1. As shown in Fig. 1(a), the rotor rotational position θ_f correnspondes to the angle difference between the center of the N-pole on the rotor and the x-axis on the stational reference frame. Let us assume the absolute position on the rotor from the x-axis on the stational reference frame as ϕ_s and the relative position on the rotor from the N-pole center as φ_r as shown in Fig. 1(b). The relation between ϕ_s and φ_r is $\phi_s = \varphi_r + \theta_f$.

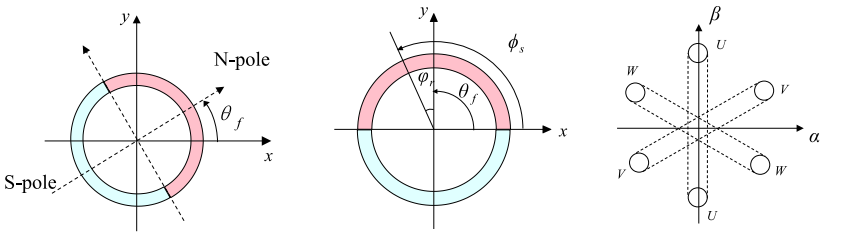

(a) The definition of rotor rotational position θ_f.

(b) The definition of the absolute position ϕ_s and the relative position φ_r.

(c) Relationship between the α-axis and the β-axis and three-phase motor windings.

Fig. 1 Definition of the reference frames and positions.

Fig.1(c) shows the definition of the α-axis parallel to the flux produced by the u-phase winding current and the β-axis orthogonal to the α-axis. The α-axis and β-axis have the same direction with the x-axis and the y-axis in the stational reference frame respectively. Next, in order to obtain the eddy current distribution on the permanent magnet, the flux density distribution is considered based on the suspension winding current and the stator permeance distribution. Let us assume the suspension winding currents are given so that the radial force is generated only in the x-direction. To apply the generalized consideration into analysis, let us introduce natural number parameter m. Both of $2m$-pole motor $2(m+1)$-pole suspension winding bearingless motors (2mt2(m+1)s BelM) and $2(m+1)$-pole motor $2m$-pole suspension winding bearingless motors(2(m+1)t2ms BelM) are analyzed in the following. Let us define the suspension winding current magnitude in the α-β axis $I_{\alpha\beta}$, three phase suspension winding currents of the 2mt2(m+1)s BelM $\boldsymbol{I}_{2m2(m+1)}$, and three phase suspension winding currents of 2(m+1)t2ms BelM $\boldsymbol{I}_{2(m+1)2m}$, $\boldsymbol{I}_{2m2(m+1)}$ and $\boldsymbol{I}_{2(m+1)2m}$ are given as shown in Eq.(1). Let us define the permeance fundamental component for 2mt2(m+1)s BelM $P_{1\,2m2(m+1)}$, for the 2(m+1)t2ms BelM $P_{1\,2(m+1)2m}$, the three phase permeance distributions $\boldsymbol{P}_{2m2(m+1)}$ and $\boldsymbol{P}_{2(m+1)2m}$ are given as the function of stator position ϕ_s shown in Eq.(2).

$$\boldsymbol{I}_{2m2(m+1)} = \sqrt{\frac{2}{3}} I_{\alpha\beta} \begin{bmatrix} \cos(m\theta_f) \\ \cos\left(m\theta_f - \frac{2}{3}\pi\right) \\ \cos\left(m\theta_f + \frac{2}{3}\pi\right) \end{bmatrix}, \quad \boldsymbol{I}_{2(m+1)2m} = \sqrt{\frac{2}{3}} I_{\alpha\beta} \begin{bmatrix} \cos((m+1)\theta_f) \\ \cos\left((m+1)\theta_f - \frac{2}{3}\pi\right) \\ \cos\left((m+1)\theta_f + \frac{2}{3}\pi\right) \end{bmatrix} \tag{1}$$

$$\boldsymbol{P}_{2m2(m+1)} = P_{1\,2m2(m+1)} \begin{bmatrix} \cos((m+1)\phi_s) \\ \cos\left((m+1)\phi_s - \frac{2}{3}\pi\right) \\ \cos\left((m+1)\phi_s + \frac{2}{3}\pi\right) \end{bmatrix}, \quad \boldsymbol{P}_{2(m+1)2m} = P_{1\,2(m+1)2m} \begin{bmatrix} \cos(m\phi_s) \\ \cos\left(m\phi_s - \frac{2}{3}\pi\right) \\ \cos\left(m\phi_s + \frac{2}{3}\pi\right) \end{bmatrix} \tag{2}$$

The suffix '2m2(m+1)'denotes 2mt2(m+1)s BelM and the suffix '2(m+1)2m' denotes 2(m+1)t2ms BelM. The flux density distribution per one phase can be given by the product of the one phase current and the one phase permeance distribution. The total flux density distribution is the resultant of each phase flux density distribution. The three-phase suspension winding current $\boldsymbol{I}_{2m2(m+1)}$, $\boldsymbol{I}_{2(m+1)2m}$ and three-phase permeance $\boldsymbol{P}_{2m2(m+1)}$, $\boldsymbol{P}_{2(m+1)2m}$ can be considered as vectors in the stational reference frame. Therefore, the flux density distribution can be derived with the inner product of the three phase current vector and the three phase permeance vector. It can be expressed as the cosine function of the phase difference between the two vectors. The flux density distribution $B_{2m2(m+1)}$ and $B_{2(m+1)2m}$ by the suspension winding current for 2mt2(m+1)s BelM and 2(m+1)t2ms BelM are derived as shown in Eq.(3) and Eq.(4) respectively.

$$B_{2m2(m+1)}(\phi_s) = \sqrt{\frac{3}{2}} I_{\alpha\beta} P_{1,2m2(m+1)} \cos((m+1)\phi_s - m\theta_f) \tag{3}$$

$$B_{2(m+1)2m}(\phi_s) = \sqrt{\frac{3}{2}} I_{\alpha\beta} P_{1,2(m+1)2m} \cos(m\phi_s - (m+1)\theta_f) \tag{4}$$

Equation (3) and (4) are the function of ϕ_s, the position from the x-axis of the stational reference frame. Since the eddy current is induced on the permanent magnet, the flux density function should be redefined on the rotational reference

frame for analytical simplicity. Substituting $\phi_s = \varphi_r + \theta_f$ in Eq. (3) and Eq. (4), the flux density distribution functions in the rotational reference frame are obtained as follows.

$$B_{2m2(m+1)}(\varphi_r) = \sqrt{\frac{3}{2}} I_{\alpha\beta} P_{1,2m2(m+1)} \cos((m+1)\varphi_r + \theta_f) \tag{5}$$

$$B_{2(m+1)2m}(\varphi_r) = \sqrt{\frac{3}{2}} I_{\alpha\beta} P_{1,2(m+1)2m} \cos(m\varphi_r - \theta_f) \tag{6}$$

From Eq.(5), it is seen that in the rotational reference frame the flux density of 2mt2(m+1)s BelM moves in the opposite direction with the rotor rotating direction. Also, from Eq. (6), the flux density of 2(m+1)s2mt BelM moves in the same direction with the rotor rotation. Let us suppose that the eddy current induced on the permanent magnet hinders the variation of suspension winding flux density, the eddy current I_e can be expressed in Eq. (7) from Eq. (5) and Eq. (6).

$$I_{2m2(m+1)} = -I_e \cos((m+1)\varphi_r + \theta_f), \quad I_{2(m+1)2m} = I_e \cos(m\varphi_r - \theta_f) \tag{7}$$

2.2. Lorentz force generated on the rotor

Next, Lorentz force generated on the rotor per unit shaft length is derived. With the interaction between the permanent magnet flux density and the eddy current, Lorentz force is generated based on Flemming's law. Let us assume the permanent magnet used in this research is magnetized parallelly. Let us define the pole number of the permanent magnet on the rotor $2p$. There are the relationship between the pole number p and the parameter m $p = m$ in the case of 2mt2(m+1)s BelM, and $p = m + 1$ in the case of 2(m+1)t2ms BelM respectively. The permanent magnet mounted on the rotor can be divided into k sections by its polarity, where $k = 0, 1, 2...2p - 1$. Let us define the start position of the k-th magnet section as $\{(2k-1)/(2p)\}\pi$, the end position of the k-th magnet section as $\{(2k+1)/(2p)\pi\}$, the flux density of the permanent magnet can be expressed as follows.

$$B_x = (-1)^k B_m \cos\left(\frac{k}{p}\pi + \theta_f\right) \tag{8}$$

$$B_y = (-1)^k B_m \sin\left(\frac{k}{p}\pi + \theta_f\right) \tag{9}$$

where B_x is the magnet flux density in the x-direction, B_y is the magnet flux density in the y-direction and B_m is the amplitude of the flux density of permanent magnets. The magnet section of $k = 0$ corresponds to the N-pole. Each time k increments, the polarity of the magnet is inverted. In this consideration the z-axis is defined as the direction from the back side of the paper to the surface of the paper. Assume that the eddy current flows only in the z-direction, Lorentz force in x-direction F_x can be calculated by the product of the flux density B_y and the eddy current and Lorentz force in y-direction F_y can be obtained with the product of B_x and the eddy current shown in Eq. (7). Lorentz forces per unit length F_x and F_y of 2mt2(m+1)s BelM and 2(m+1)t2ms BelM are given as Eq. (10), Eq. (11), Eq. (12), Eq. (13), respectively.

$$F_{x\,2m2(m+1)} = -I_{2m2(m+1)} B_y = (-1)^k I_e B_m \cos((m+1)\varphi_r + \theta_f) \sin\left(\frac{k}{p}\pi + \theta_f\right) \tag{10}$$

$$F_{y\,2m2(m+1)} = I_{2m2(m+1)} B_x = (-1)^{k+1} I_e B_m \cos((m+1)\varphi_r + \theta_f) \cos\left(\frac{k}{p}\pi + \theta_f\right) \tag{11}$$

$$F_{x\,2(m+1)2m} = -I_{2(m+1)2m} B_y = (-1)^{k+1} I_e B_m \cos(m\varphi_r - \theta_f) \sin\left(\frac{k}{p}\pi + \theta_f\right) \tag{12}$$

$$F_{y\,2(m+1)2m} = I_{2(m+1)2m} B_x = (-1)^k I_e B_m \cos(m\varphi_r - \theta_f) \cos\left(\frac{k}{p}\pi + \theta_f\right) \tag{13}$$

Lorentz force generated in the k-th section of the permanent magnet is obtained by integral calculation with respect to φ_r in Eq. (10) - Eq.(13) with the position range from $\varphi_r = \frac{2k-1}{2p}\pi$ to $\varphi_r = \frac{2k+1}{2p}\pi$. The integrated results are shown in Eq. (14)-Eq. (17).

$$\begin{aligned} F_{x,2m2(m+1)}(k) &= \int_{\frac{2k-1}{2p}\pi}^{\frac{2k+1}{2p}\pi} (-1)^k I_e B_m \cos((m+1)\varphi_r + \theta_f) \sin\left(\frac{k}{p}\pi + \theta_f\right) d\varphi_r \\ &= \frac{(-1^k) I_e B_m}{m+1} 2 \sin\left(\frac{k}{p}\pi + \theta_f\right) \cos\left(\frac{(m+1)k}{p}\pi + \theta_f\right) \sin\left(\frac{m+1}{2p}\pi\right) \\ &= \frac{I_e B_m}{m+1} \sin\left(\frac{2k}{p}\pi + 2\theta_f\right) \sin\left(\frac{m+1}{2p}\pi\right) \end{aligned} \tag{14}$$

$$
\begin{aligned}
F_{y,2m2(m+1)}(k) &= \int_{\frac{2k-1}{2p}\pi}^{\frac{2k+1}{2p}\pi} (-1)^k I_e B_m \cos((m+1)\varphi_r + \theta_f) \cos\left(\frac{k}{p}\pi + \theta_f\right) d\varphi_r \\
&= \frac{(-1^{k+1}) I_e B_m}{m+1} 2\cos\left(\frac{k}{p}\pi + \theta_f\right) \cos\left(\frac{(m+1)k}{p}\pi + \theta_f\right) \sin\left(\frac{m+1}{2p}\pi\right) \\
&= \frac{-I_e B_m}{m+1} \left\{1 + \cos(\frac{2k}{p}\pi + 2\theta_f)\right\} \sin\left(\frac{m+1}{2p}\pi\right) \qquad (15)
\end{aligned}
$$

$$
\begin{aligned}
F_{x,2(m+1)2m}(k) &= \int_{\frac{2k-1}{2p}\pi}^{\frac{2k+1}{2p}\pi} (-1)^{k+1} I_e B_m \cos(m\varphi_r + \theta_f) \sin\left(\frac{k}{p}\pi + \theta_f\right) d\varphi_r \\
&= \frac{(-1^{k+1}) I_e B_m}{m+1} 2\sin\left(\frac{k}{p}\pi + \theta_f\right) \cos\left(\frac{mk}{p}\pi - \theta_f\right) \sin\left(\frac{m}{2p}\pi\right) \\
&= \frac{-I_e B_m}{m} \sin\left(\frac{2k}{p}\pi + 2\theta_f\right) \sin\left(\frac{m}{2p}\pi\right) \qquad (16)
\end{aligned}
$$

$$
\begin{aligned}
F_{y,2(m+1)2m}(k) &= \int_{\frac{2k-1}{2p}\pi}^{\frac{2k+1}{2p}\pi} (-1)^k I_e B_m \cos(m\varphi_r + \theta_f) \cos\left(\frac{k}{p}\pi + \theta_f\right) d\varphi_r \\
&= \frac{(-1^{k}) I_e B_m}{m+1} 2\cos\left(\frac{k}{p}\pi + \theta_f\right) \cos\left(\frac{mk}{p}\pi - \theta_f\right) \sin\left(\frac{m}{2p}\pi\right) \\
&= \frac{I_e B_m}{m} \left\{1 + \cos(\frac{2k}{p}\pi + 2\theta_f)\right\} \sin\left(\frac{m}{2p}\pi\right) \qquad (17)
\end{aligned}
$$

Lorentz force on the whole of the rotor can be calculated with the sum of Lorentz force on each section expressed in Eq. (14) - Eq. (17) with substituting $k = 0, 1, 2...2p-1$.

2.3. Comparison between the different combinations of motor and suspension windings poles

In this subsection, the specific results of Lorentz force presented in the previous section with respect to 2-pole and 4-pole, and 6-pole and 4-pole of BelMs are shown. In the case of 2t4s BelM, with substituting $m = 1, p = 1$ to Eq. (14) and Eq. (15) and calculating the total amount of the each magnet section, Lorentz force of the whole rotor is calculated as shown in Eq. (18) and Eq. (19) This is the special case that both of x-direction force $F_{x,24}$ and y-direction force $F_{24,y}$ become zero because the term $\sin((m+1)/2p\pi)$ in Eq. (14) and Eq. (15) equals to $\sin(\pi)$.

$$
F_{x,24} = \sum_{k=0}^{1} \frac{I_e B_m}{2} \sin(2(k\pi + \theta_f)) \sin(\pi) = 0 \qquad (18)
$$

$$
F_{y,24} = \sum_{k=0}^{1} \frac{-I_e B_m}{2} \{1 + \cos(2(k\pi + \theta_f))\} \sin(\pi) = 0 \qquad (19)
$$

Next, with substituting $m = 1, p = 2$ to Eq. (16) and Eq. (17), Lorentz forces $F_{x,42}$ and $F_{y,42}$ of 4t2s BelM are obtained as shown in Eq.(20) and Eq.(21). Considering a symmetrical characteristic of trigonometric function, the total amount of $F_{x,42}(k)$ over the rotor circumference equals to zero. On the other hand, a constant Lorentz force in y-direction remains regardless the rotor rotational position θ_f.

$$
F_{x,42} = \sum_{k=0}^{3} I_e B_m \sin(k\pi + 2\theta_f)) \sin(\frac{1}{4}\pi) = 0 \qquad (20)
$$

$$
F_{y,42} = \sum_{k=0}^{3} I_e B_m \{1 + \cos(k\pi + 2\theta_f)\} \sin(\frac{1}{4}\pi) = 2\sqrt{2} I_e B_m \qquad (21)
$$

As regards 4t6s BelM, with substituting $m = 2, p = 2$ to Eq. (14) and Eq. (15), Lorentz forces $F_{x,46}$ and $F_{y,46}$ can be derived as shown in Eq. (22) and in Eq. (23), respectively.

$$
F_{x,46} = \sum_{k=0}^{3} \frac{I_e B_m}{3} \sin(k\pi + 2\theta_f) \sin(\frac{3}{4}\pi) = 0 \qquad (22)
$$

$$
F_{y,46} = \sum_{k=0}^{3} \frac{I_e B_m}{3} \{1 + \cos(k\pi + 2\theta_f\} \sin(\frac{3}{4}\pi) = -\frac{2\sqrt{2} I_e B_m}{3} \qquad (23)
$$

Similarly, for 6t4s BelM, with substituting $m = 2, p = 3$ to Eq. (16) and Eq. (17), the Lorentz forces $F_{x,64}$ and $F_{y,64}$ can be derived as shown in Eq. (24) and in Eq. (25), respectively.

$$F_{x,64} = \sum_{k=0}^{5} I_e B_m 2 \sin(\frac{2k}{3}\pi + 2\theta_f) \sin(\frac{1}{4}\pi) = 0 \tag{24}$$

$$F_{y,64} = \sum_{k=0}^{5} \frac{I_e B_m}{2} \{1 + \cos(\frac{2k}{3}\pi + 2\theta_f)\} \sin(\frac{1}{4}\pi) = \frac{3\sqrt{3} I_e B_m}{2} \tag{25}$$

3. FEM simulation results and discussion

3.1. FEM simulation conditions

In this section firstly the conditions used in the FEM simulation and the analytical calculations are presented. The parameters of the evaluated bearingless motors used in the FEM simulation are shown in Tables 1 and 2. In this evaluation the permanent magnet is magnetized parallelly. Figs. 2(a)-(d) show the x-direction and the y-direction flux density on the rotor permanent magnet of 2t4s BelM, 4t2s BelM, 4t6s BelM and 6t4s BelM, respectively. The horizontal axis indicates the position on the rotor φ_r. As shown in Fig.2(a) the average flux density B_x of 2t4s BelM is 0.732[T]. The average flux densities B_x in the position range from 0 [deg] to 45 [deg] of 4t2s BelM and 4t6s BelM are 0.827[T] and 0.600[T] respectively. The average flux density of 6t4s BelM in the position range from 0 [deg] to 30 [deg] is 0.588[T]. These average value is used as the flux density B_m in the analytical calculations. The current references to the suspension windings are given so that the x-direction radial force can reach 65[N] in the all types of evaluated motors. In the following consideration, 65[N] is assumed as the 100% radial force. In the analytical calculation Eq. (18) - Eq. (25), the magnitude of the eddy current is needed. Then, the eddy current magnitude is calculated with the fundamental component of averaged current density distribution in the permanent magnet obtained by the FEM simulation and the cross-sectional area of the permanent magnet. 2-D FEM simulations are conducted with JMAG ver. 23 (JSOL Corporation).

3.2. FEM simulation results

Figs. 3(a)-(d) show Lorentz force computed with the FEM simulation and the analytical calculation results with Eq.(18) - Eq.(25) in the speed range from 6000 [r/min] to 12000[r/min].

Table 1 Common paramters of 2t4s BelM and 4t2s BelM.

Stator core	50A600	Outer diameter 120 mm Inner diameter 62 mm
Rotor core		Outer diameter 46 mm
Permanent magnet	N45H	Thickness 5.0 mm
Airgap length		3.0 mm

Table 2 Common paramters of 4t6s BelM and 6t4s BelM.

Stator core	50A600	Outer diameter 120 mm Inner diameter 80 mm
Rotor core		Outer diameter 64 mm
Permanent magnet	N45H	Thickness 5.0 mm
Airgap length		3.0 mm

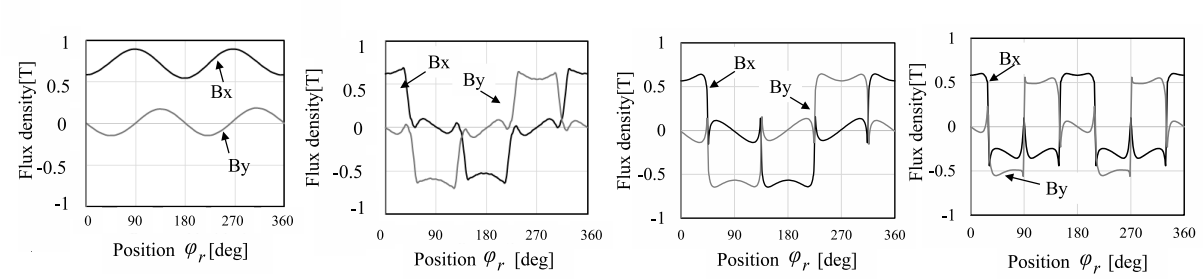

(a) Magnet flux density of 2t4s BelM

(b) Magnet flux density of 4t2s BelM

(c) Magnet flux density of 4t6s BelM

(d) Magnet flux density of 6t4s BelM

Fig. 2 Permanent magnet flux density B_x and B_y distribution on the rotor.

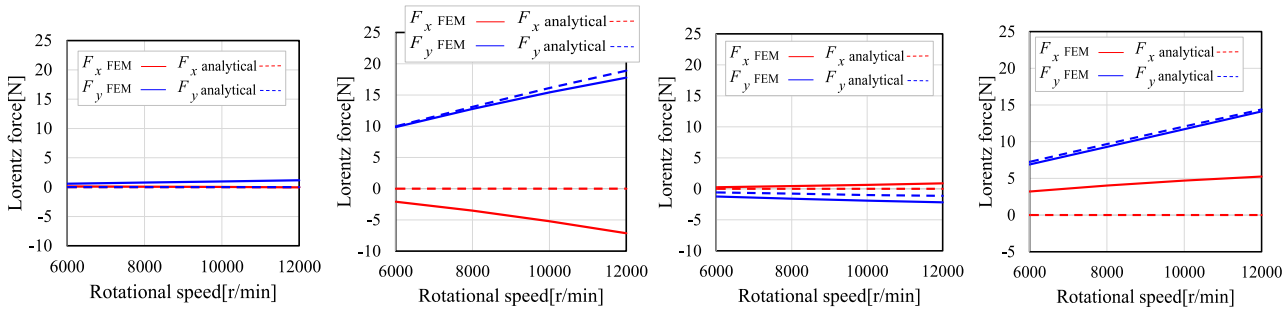

(a) 2t4s BelM (b) 4t2s BelM (c) 4t6s BelM (d) 6t4s BelM

Fig. 3 Lorentz force versus the rotor rotating speed.

In Figure. 3, the red lines and blue lines represent F_x and F_y respectively. Also, solid lines indicate the FEM simulation results and dashed lines indicate the analytical calculation results. As shown in Fig.3(a), in the case of 2t4s BelM, FEM simulation result shows that F_x is less than 0.65[N](1% of 65[N]) in the all speed range and the maximum F_y is 1.18[N](1.8%) at 12000[r/min]. Therefore, the analytical calculation results with Eq. (18) and Eq. (19) are close to the FEM simulation results in this case. Similarly, in the case of 4t6s BelM, the differences between the analytical calculation with Eq.(22) and Eq.(23) and the FEM simulation are 0.88[N](1.35%) in F_x and 1.05[N](1.61%) in F_y as shown in Fig.3(c). In the cases of 4t2s BelM and 6t4s BelM, the FEM simulation results and the analytical calculation results regarding F_y almost agree. However, in x-direction, the significant errors between the analytical calculation and the FEM simulation appears. As shown in Fig.3 (b) and (d), the x-direction forces reach to -7.13[N](10.9%) in 4t2s BelM and 5.25[N](8.1%) in 6t4s BelM at 12000 [r/min], respectively.

3.3. Discussion

In this section, the cause of Lorentz force in x-direction generated in 4t2s BelM is discussed with focusing on the eddy current variation. Figure. 4 shows the current density distribution on the permanent magnet computed with FEM simulation at the range from 6000 [r/min] to 12000 [r/min]. The horizontal axis indicates the position on the rotor φ_r. The positive phase angle corresponds to the counter-clockwise direction. It can be seen that the phase angle of the current density on the rotor shifts in proportion to the rotational speed. Considering the route eddy current flows, eddy current has no divergence (Takahashi and Kurita, 1988) . Therefore, the voltage drop in the resistance component and the electromotive force induced by the time variation of the flux density are in equilibrium. Let us assume the reflective flux density produced by eddy current B_e, the flux density produced by the suspension winding current B_s, the conductivity σ, the eddy current density$\boldsymbol{j_e}$ is given by the following equation.

$$curl(\boldsymbol{j_e}) = -\sigma\left(\frac{\partial B_s}{\partial t} + \frac{\partial B_e}{\partial t}\right) \tag{26}$$

According to (Takahashi and Kurita, 1988) , it is possible to express the reflective flux density distribution B_e as a function of eddy current density utilizing the calculation results with Biot-savart's law. In this consideration, let us assume the reflective flux density B_e can be expressed approximately as a function of the position differential of the eddy current density. Let us define the coefficient K_{Be}, the rotor radius r, the amplitude of the current density J_{em}, the reflective flux density produced by eddy current B_e can be estimated as shown in Eq. (27).

$$B_e = K_{Be}\frac{1}{r}\frac{\partial \boldsymbol{j_e}}{\partial \varphi_r} = K_{Be}\frac{J_{em}}{r}\sin(\varphi_r - \omega t + \alpha) \tag{27}$$

where, ω is the rotational angular speed, α is the phase difference between the suspension winding flux density B_s and eddy current density. Let us suppose that the eddy current distribution conforms to Eq.(7). The relationship among B_e , B_s and the eddy current is rewritten with Eq.(7), Eq.(26) and Eq.(27) as shown in Eq. (28).

$$-\frac{J_{em}}{r}\sin(\varphi_r - \omega t + \alpha) = -\sigma\{\omega B_{sm}\sin(\varphi_r - \omega t) + \omega K_{Be}\frac{J_{em}}{r}\cos(\varphi_r - \omega t + \alpha)\} \tag{28}$$

where, B_{sm} is the amplitude of the flux density by suspension winding current. In Eq. (28), the left term corresponds to $curl(\boldsymbol{j_e})$ in Eq. (26) and the right terms correspond to the time variation of B_s and B_e. With transposing the second right

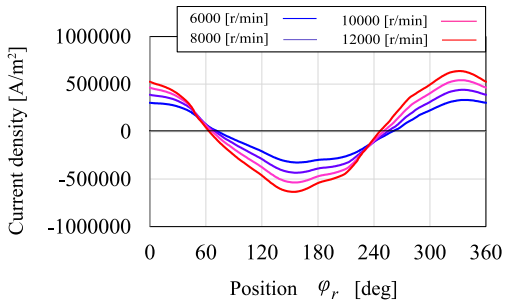

Fig. 4 The eddy current density.

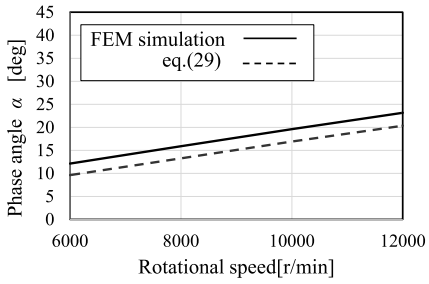

Fig. 5 The phase angle of the eddy current α.

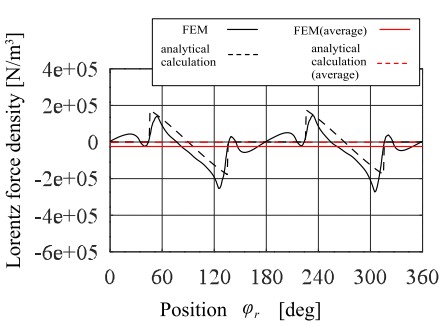

(a) 6000 [r/min]

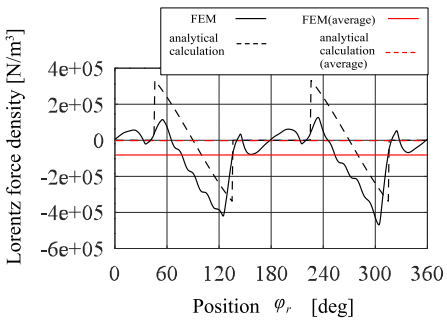

(b) 12000 [r/min]

Fig. 6 The Lorentz force density versus position φ_r.

term in Eq.(28) to the left term, Eq.(28) can be modified shown as Eq. (29).

$$\frac{J_{em}}{r}\sqrt{1+(\sigma\omega K_{Be})^2}\sin(\varphi_r-\omega t+\alpha+\arctan(-\sigma\omega K_{Be}))=\sigma\omega B_{sm}\sin(\varphi_r-\omega t) \tag{29}$$

Equation (29) has to be a identical equation. Consequently, the phase angle α has to be equal to $\arctan(\sigma\omega K_{Be})$. Next, in order to confirm the effect of the reflective flux density produced by the eddy current, the calculation to obtain the phase angle α is attempted with the 4t2s BelM model. The coeffient K_{Be} can be estimated by the correlation between the eddy current density and the flux density B_e. In the low speed region, the reflective flux density B_e by the eddy current can be disregarded. Then, the estimated B_e is obtained with the difference between suspension current flux density B_s at the high speed range(6000-12000 [r/min]) and B_s at the low speed range(1000[r/min]). The coefficient K_{Be} is calculated with the fundamental component of the estimated B_e and the eddy current density amplitude I_e. The estimated K_{Be} is 4.4×10^{-10}. Then, with utilizing the results of the FEM simulation, the eddy current phase angle α is compared with FEM simulation and calculation result with Eq. (29). Figure. 5 shows the calculation results of the estimated phase angle α. It can be seen that the both calculated results have similar inclination to the rotational speed and the offset between the two calculation results is less than 5[deg]. From this result, it is considered that the eddy current phase shift is affected by the reflective flux density B_e. Next, It is explained how the negative Lorentz force is produced when the eddy current phase shifts. Figs. 6(a) and (b) show the Lorentz force density at rotational speed 6000 [r/min] and 12000[r/min] respectively. The horizontal axis corresponds to the position on the rotor φ_r. The FEM simulation results and the analytical calculation results based on Eq.(12) are depicted in solid line and dashed line respectively. It can be seen that the average values of FEM simulation results have negative value. On the other hand, the average value of the analytical calculation is zero. The phase angle of the eddy current in the FEM simulation are 12.1 [deg] at 6000 [r/min] and 23.2 [deg] at 12000 [r/min]. The eddy current phase used in the analytical calculation is set to zero. Since Lorentz force is the product of the current and flux density, it is considered that the eddy current phase shift in the clockwise direction occurs the negative offset of Lorentz force in x-direction. With respect to 6t4s BelM, a non-negligible magnetic saturation influence is observed in the evaluated motor model used in this research. The cause of F_x of 6t4s BelM will be investigated in the future work after the problems caused by magnetic saturation are solved.

4. Conclusion

Based on the flux density distribution produced by the suspension winding current, the Lorentz force generation

models of the 2mt2(m+1)s Bearingless SPM and 2(m+1)2m Bearingless SPM are derived when the suspension winding current reference is commanded to generate the radial force in the *x*-direction. The analytical calculation results show that the Lorentz forces appear in the *y*-direction in all types of BelM except 2t4s BelM. 2t4s BelM is the special case in which Lorentz forces produced in two magnets are canceled each other. To confirm the effectiveness the derived model, the FEM simulation is conducted using 2-pole and 4-pole, and 6-pole and 4-pole bearingless motors. The results of the analytical calculation and the FEM simulation are close in the case of the *y*-direction. However, the *x*-direction Lorentz force, which are equals to zero in the analytical calculation, are produced approximately 10% of the rated radial force. The cause of the *x*-direction Lorentz force is investigated with respect to 4t2s BelM additionally. With taking the reflective magnetic field produced by eddy current to consideration, the phase angle is estimated based on the relation between the eddy current differential function and reflective flux density. The estimated phase angle of the eddy current shifts in the clockwise direction on the rotor by the influence of the reflective flux density in propotion to the rotational speed. It is confirmed with FEM simulation that the negative Lorentz force is generated as the eddy current phase angle shifts in the high speed range.

References

Fukushima, T., Ooshima, M., Combination of pole number of motor and suspension windings and the influence on suspension force in bearingless motors , *ICEMS 2020*(The 23rd International Conference on Electrical Machine and Systems), LS1C-2, 2020.

Liu, Z., Chiba, A., Irino, Y., Nakazawa, Y., Optimum pole number combination of a buried permanent magnet bearingless motor and test results at an output of 60kW with a speed of 37000 r/min, *IEEE Open J. Ind. Appl.*, vol.1 pp. 33-41, Feb. 2020.

Okada, Y., Dejima, K., Ohishi, T., Analysis and comparison of PM synchronous motor and induction motor type magnetic bearings, *IEEE Trans. on Ind. Appl.*, vol. 31, no. 5, Sept./Oct., 1995.

Noguchi, T., Sugimoto, H., Fujii, Y., Chiba, A., Verifying Calculation Approach of Radial Suspension Force based on the Airgap Flux Density for SPM, Consequent-Pole, and Bearingless AC Homopolar Motors, IEEJ Trans. IA, vol. 142, no. 7, pp. 506- pp.515, 2022. (in Japanese)

Takahashi, T., Kurita, K., Computation of eddy current induced in a conducting sheet under moving magnets, IEEE Transactions on Magnetics, vol. 24, no. 1, pp.197-pp. 200, 1988.